Diamond nanowires with nitrogen vacancy under a transverse electric field

Jihua Zhang, J. X. Cao, Xiaoyuan Chen, J. W. Ding, Peihong Zhang, and Wei Ren

Phys. Rev. B **91**, 045417 — Published 13 January 2015

DOI: 10.1103/PhysRevB.91.045417

Diamond Nanowires with Nitrogen-Vacancy under a Transverse Electric Field

Jihua Zhang[1,2] , J. X. Cao[1] , Xiaoyuan Chen[3], J. W. Ding[1,*], Peihong Zhang [4,5], Wei Ren[5,*]

1 Department of Physics, Xiangtan University, Xiangtan 411105, China
2 Guizhou Provincial Key Laboratory of Computational Nano-Material Science, Guizhou Normal College, 115 Gaoxin Road, Guiyang, 550018, China
3 Shanghai Advanced Research Institute, Chinese Academy of Sciences, 99 Haike Road, Shanghai 201210, China
4 Department of Physics, University at Buffalo, State University of New York, Buffalo, New York 14260, USA
5 International Centre for Quantum and Molecular Structures and Department of Physics, Shanghai University, 99 Shangda Road, Shanghai 200444, China
* jwding@xtu.edu.cn, renwei@shu.edu.cn

Abstract: We have investigated the electronic, magnetic and optical properties of hydrogenated diamond nanowires (DNW) with nitrogen-vacancy (NV) centers using density functional theory (DFT). The strong localization of defect states results in the formation of local magnetic moments with a spin polarization energy that is close to those for transition metal atoms. Such spin-polarized defect states are found to be stable well above room temperature, in agreement with previous experimental reports. In addition, we find that a semiconductor-metal transition can be triggered upon applying a transverse electric field. Furthermore, an enhanced optical absorption in the visible-light region is predicted in DNW with NV centers. The strength and the position of the absorption can be tuned or optimized by an external electric field and/or the nanowire diameter.

PACS: 81.05.uj, 31.15.A-, 75.75.-c, 78.67.-n

1. Introduction

The successful synthesis of diamond nanowires (DNW) using an atmospheric pressure chemical vapor deposition (CVD) process [1] adds a brand new member to the family of nanocarbon. The electronic structure of DNW is significantly different from that of bulk diamond thanks to the quantum confinement and dimensionality effects. Barnard *et al.*[2] showed that the band gaps of DNW could be significantly smaller than that of bulk diamond due to the introduction of surface states. Recent advances in synthesis, characterization, and structural modification techniques have demonstrated new promises of DNW, where defects can play an important and often beneficial role. Specifically, the nitrogen-vacancy (NV) color center in nanodiamond, consisting of a substitutional nitrogen (N) and a carbon vacancy (V) at an adjacent lattice site, has been investigated for a wide range of applications in quantum information processing[3, 4]. The NV center occurs in several different charged states, with the neutral (NV^0) and the negatively charged (NV^-) states being the most stable ones. NV^- is the prevailing state for centers buried deep inside bulk diamond. However, they become unstable and turn into NV^0 near the surface[5] as well as in nanodiamonds[6, 7]. Recently, Bradac *et al.*[6] have observed NV centers in 5-nm nanodiamonds at room temperature. Hydrogenated DNW of even smaller diameters could also be realized with the development of nanowire technology. Therefore, we will focus on NV^0 centers in ultrasmall-diameter DNWs in this paper.

In addition to their potential in quantum information processing, NV centers in nanodiamonds are also very promising for room temperature magnetic imaging and

spectroscopy. Understanding magnetism at the nanoscale is very important for fundamental physics as well as for enabling critical ingredients for data storage and spintronic devices[8]. Balasubramanian *et al.*[9] have demonstrated the synthesis and application of ultrapure isotopically controlled single-crystal CVD diamond nanocrystals with a remarkably low concentration of paramagnetic NV centers. It was recognized that the magnetic properties of these defects in nanodiamond can be used for novel microscopy [8, 10-13]. Compared with other systems used for nanoscale magnetic imaging, NV centers based scanning probes stand out owing to their excellent photo and chemical stabilities that allow operations at room temperature or even under harsh conditions. Despite intensive research, the physics of the unique magnetic states of NV in DNW is not yet fully understood.

In the past few years, electric field has been shown as a promising means to modulate the electronic structure and optical properties of nanoscale materials [14-16]. Tamarat *et al.*[17] find that an external electric field can be used to control the optical properties of a single NV center in diamond. Stark shifts at low temperature have been demonstrated in the excited triplet states of single defects[18] and the ground state of NV ensembles[19]. It is noted that spectral tuning of the spin-selective optical transition by an external electric field is a first step toward controlled optical dipole coupling between close NV centers in nanodiamond[18]. The application of finer nanometer sized gates and possibly feedback control of the applied voltage will pave the way toward optical control of the spin state of NV centers.[18]. Dolde *et al.*[20] introduced a quantum-metrology technique demonstrating precision

three-dimensional electric-field (produced by an elementary charge) measurement using the spin of a single NV center in diamond. Since the electronic structure and optical properties of DNWs can be tuned by either size effect and/or transverse electric field, it is thus very important to understand their cooperation as presented in our work.

In this paper, we present a detailed first-principles investigation on the electronic, magnetic and optical properties of hydrogenated DNWs with NV centers. We find that the properties of NV doped DNW can be controlled/tuned by applying an external electric field and/or varying the nanowire diameter. The paper is organized as follows. Section 2 describes the computational models and methods. In Section 3, we present the electronic, magnetic, and optical properties of NV doped DNWs, focusing on size-dependence and the effects of the electric field on the tuning of these properties. We conclude and summarize our work in the Section 4.

2. Models and methods

Experimentally, the {111} nanowires were most commonly observed[21, 22]. It was also observed that under certain growth conditions, the growth rates along the {100} and {110} directions may prevail over the {111} ones[23]. The growth directions of the DNWs are affected by several factors including the substrate surface and gas pressure[23, 24] and energetics is not the sole factor controlling the growth of DNWs. Theoretically, heat of formation (Hf) can be used to characterize the relative stability of nanostructures[25, 26] and to further reveal the preferential growth orientation of

nanowires[27]. For examples, Zhao[28] et al found that all DNWs except {110} ones are thermodynamically stable with a negative Hf. This was also observed in the unpassivated DNWs[29]. Therefore we focused only on nanowire structures "cleaved" from bulk diamond with C{100} dangling bonds on the surfaces. This model is in consistent with the previous report[29]. The dangling bonds are then passivated with atomic hydrogen atoms. Experimentally, atomic hydrogen is instrumental in enhancing the yield of DNW[1].

The structure of a hydrogenated DNW with C {100} surfaces is shown in Fig. 1(a). The primitive cells of DNWs of various sizes investigated in this work are denoted as C_9H_{12}, $C_{16}H_{16}$, $C_{25}H_{20}$, $C_{36}H_{24}$, $C_{49}H_{28}$, $C_{64}H_{32}$ and $C_{81}H_{36}$, with a general formula $C_{n\times n}H_{4n}$ (n=3,4,5,6,7,8,9). An NV center is then introduced into the (1×1×2) supercell of the nanowire primitive cells. The NV-containing DNWs are denoted as NV:$C_{48}H_{40}$, NV:$C_{70}H_{48}$, etc., with a general formula $C_{2n\times n-2}H_{8n}$. The three C atoms near the substitutional N atom are labeled as A1, A2 and A3, respectively, as shown in Fig. 1(b). We find that qualitative features of the electronic structure are not sensitive to the diameter of the DNW.

All calculations are carried out using the VASP code[30] with the projector augmented wave approach[30] to describe the ion-electron interactions. Since the local density approximation (LDA) or the generalized gradient approximation (GGA) approach usually underestimates the band gap of semiconductors, we use the screened hybrid functional of Heyd, Scuseria, and Ernzerhof (HSE) [31] in this work for a more accurate description of the electronic structure and optical properties. It is well-known

that the long-range Coulomb interaction in unscreened hybrid functionals such as the PBE0[32] functional gives rise to a number of numerical and theoretical difficulties [33] when they are applied to extended systems. Much of the difficulty is alleviated with the use of a screened (therefore short-ranged) Coulomb potential. In this work, we use the HSE06 functional [31] with an HF mixing $\alpha = 25\%$ and a screening parameter $\omega = 0.2\text{Å}^{-1}$. A plane wave cutoff of 450 eV is used for expanding the wave functions. Using this functional, the calculated lattice constant of bulk diamond is 0.3547 nm, which compares well with the experimental value of 0.3556 nm[34]. The calculated band gap (5.46 eV) also agrees with experiment (5.5 eV)[35].

The Brillouin-zone (BZ) integration is carried out using the k-point sampling method of Monkhorst-Pack [36] with a density of 1×1×6 and 1×1×4 for pure DNW and NV doped DNW, respectively. A simple Gaussian smearing scheme with a smearing parameter of 0.05 eV is used in all calculations. We have also tested other smearing methods such as that of Methfessel and Paxton[37] and find that the results are consistent with those obtained with the Gaussian smearing. The external electric field is introduced by adding a planar dipole layer in the middle of the vacuum part in the periodic supercell[38] as implemented in VASP. All atoms are fully relaxed without the external field until the maximum magnitude of the force acting on the atoms is smaller than 0.02 eV/Å.

The DNW axis is oriented along the *z* direction and the external electric field is along the *x* direction with an increment of 0.2 V/Å. The effects of the applied electric field on the atomic structure are neglected as they are very small. A dipole

correction[39] is applied in calculations with external field to remove interactions with periodic dipole images.

The imaginary part $\varepsilon_2(\omega)$ of the dielectric function $\varepsilon(\omega)$ is calculated using the standard formulation:

$$\varepsilon_2 = \frac{Ve^2}{2\pi\hbar m^2\omega^2}\int d^3\mathbf{k}\sum_{n,n'}\left|\left\langle \boldsymbol{k}n\left|\mathbf{p}\right|\mathbf{k}n'\right\rangle\right|^2 \times f(\mathbf{k}n)\left(1-f\left(\mathbf{k}n'\right)\right)\delta\left(E_{\mathbf{k}n}-E\mathbf{k}n'-\hbar\omega\right), \quad (1)$$

where $\hbar\omega$ is the energy of the incident photon, $\mathbf{p}$ is the momentum operator ($\hbar/i$)($\partial/\partial x$), ($|\mathbf{k}n\rangle$) is the electronic wave function, and f ($\mathbf{k}n$) is the Fermi function. The real part $\varepsilon_1(\omega)$ is related to $\varepsilon_2(\omega)$ by the Kramer–Krönig transformation. The refractive index $n(\omega)$ and absorption coefficient $I(\omega)$ can be derived from $\varepsilon_1(\omega)$ and $\varepsilon_2(\omega)$ as follows[40]

$$n(\omega) = [\sqrt{\varepsilon_1^{\,2}(\omega)+\varepsilon_2^{\,2}(\omega)}+\varepsilon_1(\omega)]^{1/2}/\sqrt{2}\,, \quad (2)$$

$$I(\omega) = \sqrt{2}\omega\left[\sqrt{\varepsilon_1^{\,2}(\omega)+\varepsilon_2^{\,2}(\omega)}-\varepsilon_1(\omega)\right]^{1/2}. \quad (3)$$

3. Results and discussion

3.1 Electronic and magnetic properties

For hydrogenated DNWs without defects, the quasi-1D confinement effect results in an increased band gap with reducing nanowire cross-sectional area. Figure 1(c) shows the size-dependence of the band gap (blue curve) as well as the axial lattice constant (red curve) of DNW. The significant reduction of the band gap of the hydrogenated DNW (compared with bulk diamond) is due to surface states and is consistent with previous results[2, 28]. Also we note that due to the HSE06 hybrid exchange-correlation functional used in the present study, all the band gaps are

systematically larger than previous GGA results[2, 28], therefore a better comparison with the experimental result can be expected. The overall size-dependence trend, however, is unchanged. The lattice constant *c* of NDW elongates significantly compared with the ideal diamond lattice parameter due to surface tension effects. This elongation is the largest (about 4.4%) for the smallest DNW and decreases with increasing NDW cross-sectional area. Figure 1(d) shows the calculated DOS (black solid line) for NV:$C_{160}H_{72}$, along with the projected DOS (blue dotted line) onto carbon *p* orbitals. Three NV-derived defect states inside the band gap can be easily identified. The degeneracy of NV-derived *E* state in bulk diamond is removed, and the unoccupied split-off majority *E* state, as well as minority *E* states, merges into low energy conduction states. The strong spin polarization results in a large splitting between the majority and minority spin states and the formation of a local moment of 1.0 μ_B (to be compared with 2.0 μ_B for negatively charged NV centers[41]). This is because localization of defect states may favor spontaneous spin polarization and the formation of local magnetic moments[42]. Moreover, atomic spin polarization of *p* orbitals is very strong for light atoms such as C, N, and O, for which the spin polarization energy is close to those of transition metal atoms[43]. The spin-polarization energy E^{pol} of NV:$C_{160}H_{72}$, defined as the energy difference between the spin-polarized and spin-unpolarized states, is about −0.36 eV. Note that the spin polarized state is stable if $E^{pol} < 0$. Therefore, we conclude that the spin polarized state of NV:$C_{160}H_{72}$ should be stable well above room temperature in agreement with previous experimental reports[8, 10-12, 44].

The localization of the defect states in these systems can also be visualized by plotting the charge density of defect states in the real space. Figure 1(b) shows an isosurface (with ρ = 0.02 e/Å^3) plot of the spin density [ρ(up) − ρ(down)] for NV:$C_{160}H_{72}$. It is evident that these defect states are strongly localized near the three C atoms surrounding the C vacancy. It is this strong localization of defect wavefunctions that leads to a stable spin-polarized ground state in these systems. Similar to the cation vacancy in III-nitrides [45], the extended tails of the defect wavefunctions might mediate a long-range magnetic coupling between defect-induced local moments. We make use of the Bader topological density analysis[46] to calculate the contribution to the total magnetic moment from each atom within an extended solid. The magnetic moments of NV:$C_{160}H_{72}$ for A1, A2 and A3 atoms in Fig. 1(b) are about −0.54 μ_B (minority-spin), 0.65 μ_B (majority-spin) and 0.65 μ_B (majority-spin), respectively.

3.2 Electronic and magnetic properties with the presence of an external electric field

Now we turn our attention to the effects of a transverse electric field on the electronic and magnetic properties of DNW. Figure 2 shows the DOS of NV:$C_{160}H_{72}$ under external electric fields $\vec{E}$ of 0.1, 0.3, 0.5, and 0.7 V/Å. As the field strength increases, the low energy conduction states move from 1.83 eV towards the Fermi level at 0 eV. We mention that strong Stark effects have been observed experimentally[17, 18, 20]. The moderate external electric field has minor effects on the carbon derived valence states. When the electric field is increased to 0.7 V/Å, the

majority spin defect state near the Fermi level merges with conduction states. This suggests an interesting electric-field induced insulator-metal transition mechanism in these systems. The electric field induced insulator-metal transition is a result of the different electronic polarizability of delocalized surface states (conduction bands) and localized defect and valence states. The delocalized states are more polarizable therefore are significant affected by the applied field. It is this contrasting response to the applied field by delocalized and localized states that is responsible for the observed field-induced insulator-metal transition.

Figure 3 shows the electric-field dependent local magnetic moments of the three carbon atoms near the NV center. Below the critical field strength, the magnetic property is insensitive to the $\vec{E}$ field. When the strength of the electric field is increased beyond the critical field of 0.7 V/Å, the total magnetic moment starts to decrease. This is because when the conduction band drops (as a result of the applied field) to close to defect states, electrons start to occupy conduction bands, thus reducing the spin polarization of the defect states. Further increasing the applied electric field beyond the critical field (~ 0.7 V/Å) would then drive one of the majority-spin defect states to be above the conduction band. When this majority-spin defect state is well above the CBM state, it is then completely unoccupied, and the total moment disappears since the spin-up and spin-down defect states are now evenly occupied.

3.3. Optical properties of diamond nanowires with and without NV centers

The size-dependent static refractive $n(0)$ along the [001] direction is show in Fig.

4(a). The refractive index increases with the lateral size of the hydrogenated DNW, ranging from 1.2 for the smallest and 1.5 for the largest DNW studied. These results are in good agreement with the previous experimental reports [47-49] and are consistent with the observation that a significant enhancement in the collection efficiency of the single-photon emission in the DNW geometry is due to the reduced refractive index in these system compared to that of the bulk diamond (n = 2.4) [50]. Similar size effects are observed for pure DNW, NV-doped DNW, and NV-DNW under electric field as shown in Fig. 4(a). In the following, we investigate the absorption coefficient of DNWs with NV doping and under an external electric field.

In Figure 4(b), we show the absorption coefficients along the [001] direction between 0 and 4 eV for $C_{49}H_{28}$, $C_{64}H_{32}$, $C_{81}H_{36}$, NV:$C_{96}H_{56}$, NV:$C_{128}H_{64}$ and NV:$C_{160}H_{72}$. The in-gap defect states give rise to a broad absorption from 2.5 to 3.5 eV. This significantly red-shifted [indicated by a red arrow in Fig. 4(b)] optical absorption is a result of optical transitions between defect states and conduction bands, and is not sensitive to the diameter of DNW. The absorption coefficient of NV:$C_{96}H_{56}$ exhibits one main peak at about 3.31 eV, and those for NV:$C_{128}H_{64}$ and NV:$C_{160}H_{72}$ peak at about 3.26 eV. Doping with NV centers thus has a much stronger effect on the optical properties of DNW than the size effect. As a result, the NV doping shall have an important impact on the photocatalytic activity of diamond nanowires and might make them potential candidates for photoelectrochemical applications. Meanwhile, because the ultraviolet (UV) absorption is also substantially enhanced, NV doping in diamond nanowires may find their uses in short-wavelength optoelectronic devices,

such as UV detectors and UV light emitting diodes (LEDs).

The calculated absorption coefficients along the [001] direction for NV:$C_{160}H_{72}$ under external transverse electric fields $\vec{E}$ of 0, 0.1, 0.3, 0.5, 0.7 V/Å are shown in Fig. 4(c). As the electric field strength increases, the absorption coefficients in the visible light region is enhanced considerably. For $\vec{E}$ = 0.7 V/Å, three additional peaks appear at 1.81 eV, 2.66 eV, and 2.81 eV. These lower energy absorption peaks are a result of the strong Stark effect of the conduction bands discussed earlier. These results suggest an interesting and effective mechanism for active-tunings of optical absorption via external fields.

Finally, we investigate the combined size and electric field effects on the optical properties of NV-doped DNW. The absorption coefficients of NV:$C_{96}H_{56}$, NV:$C_{128}H_{64}$ and NV:$C_{160}H_{72}$ under external electric field $\vec{E}$ of 0 and 0.7 V/Å are presented in Fig. 4(d). As it is already shown in Fig. 4(b), NV-doping can cause a significant red-shift to the optical adsorption edge, thus increasing the absorption in the visible light region although the main absorption still locates in the UV region. With the application of an external electric field of 0.7 V/Å, absorption peaks are moved into visible light region, at 2.77 eV, 2.68 eV, and 2.65 eV for NV:$C_{96}H_{56}$, NV:$C_{128}H_{64}$ and NV:$C_{160}H_{72}$, respectively. The magnitude of the absorption peak is also dependent on the size of DNW. Therefore, we find that the positions of absorption peaks mainly depend on the doping effect and external electric field, while the strength of the peak absorption is mainly determined by the size (diameter) effect. These results suggest that the optical absorption of DNW can be remarkably

modulated by size effect, doping effect and external electric field, thus offering multidimensional, combined active and passive tuning and optimization of the optical properties of NV-doped DNW for specific applications.

4. Summary

In summary, we present a detailed first-principles investigation on the electronic, magnetic and optical properties of DNW doped with NV centers. The strong localization of defect states results in spontaneous spin polarization and local moment formation upon NV doping. The spin-polarized state of the doped system should be stable well above room temperature, consistent with previous experimental reports. A semiconductor-metal transition is predicted in NV doped DNW systems under a moderate external electric field. This is a result of contrasting Stark effects on the conduction states and valence and defect states. Our results should be valid provided that the size of the nanowire is large enough to confine the defect states, and to support delocalized surface states. A strong optical absorption in the visible-light region is observed for NV-doped DNWs. Whereas the position of the absorption peaks can be actively tuned by the external electric field, the strength of the peak absorption can be controlled by the diameter of the DNW. Our results suggest that NV-doped diamond nanowires may provide new opportunities for short-wavelength optoelectronic devices and photoelectrochemical applications.

Acknowledgements

This work was supported by National Key Basic Research Program of China (Grant No. 2015CB921600), National Natural Science Foundation of China (Nos.

11374252, 11274222 and 11328401) scientific research fund of GPED (No. 2114118006zx) and the GZNC startup package (No. 13BS027). We also acknowledge QiMingXing Project (14QA1402000) from Shanghai Municipal Science and Technology Commission, Shanghai Shuguang Program (12SG34) and the Eastern Scholar Program from Shanghai Municipal Education Commission, Shanghai Supercomputer Center and Research Center of Supercomputing Application at National University of Defense Technology. Work at UB is also supported by the US Department of Energy under Grant No. DE-SC0002623.

References

1. C.-H. Hsu, S. G. Cloutier, S. Palefsky and J. Xu, Nano Lett. **10**, 3272 (2010).
2. A. S. Barnard, S. P. Russo and I. K. Snook, Phys. Rev. B **68**, 235407 (2003).
3. D. DiVincenzo, Nat. Mater. **9**, 468 (2010).
4. L. Childress, M. V. Gurudev Dutt, J. M. Taylor, A. S. Zibrov, F. Jelezko, J. Wrachtrup, P. R. Hemmer and M. D. Lukin, Science **314**, 281 (2006).
5. K. M. C. Fu, C. Santori, P. E. Barclay and R. G. Beausoleil, Appl. Phys. Lett. **96**, 121907 (2010).
6. Bradac C., GaebelT, NaidooN, M. J. Sellars, TwamleyJ, L. J. Brown, A. S. Barnard, PlakhotnikT, A. V. Zvyagin and J. R. Rabeau, Nat. Nanotechnol. **5**, 345 (2010).
7. L. Rondin, G. Dantelle, A. Slablab, F. Grosshans, F. Treussart, P. Bergonzo, S. Perruchas, T. Gacoin, M. Chaigneau, H. C. Chang, V. Jacques and J. F. Roch, Phys. Rev. B **82**, 115449 (2010).
8. C. L. Degen, Appl. Phys. Lett. **92**, 243111 (2008).
9. G. Balasubramanian, P. Neumann, D. Twitchen, M. Markham, R. Kolesov, N. Mizuochi, J. Isoya, J. Achard, J. Beck, J. Tissler, V. Jacques, P. R. Hemmer, F. Jelezko and J. Wrachtrup, Nat. Mater. **8**, 383 (2009).
10. L. Rondin, J. P. Tetienne, P. Spinicelli, C. Dal Savio, K. Karrai, G. Dantelle, A. Thiaville, S. Rohart, J. F. Roch and V. Jacques, Appl. Phys. Lett. **100**, 153118 (2012).
11. J. M. Taylor, P. Cappellaro, L. Childress, L. Jiang, D. Budker, P. R. Hemmer, A. Yacoby, R. Walsworth and M. D. Lukin, Nat. Phys. **4**, 810 (2008).
12. G. Balasubramanian, I. Y. Chan, R. Kolesov, M. Al-Hmoud, J. Tisler, C. Shin, C. Kim, A. Wojcik, P. R. Hemmer, A. Krueger, T. Hanke, A. Leitenstorfer, R. Bratschitsch, F. Jelezko and J. Wrachtrup, Nature **455**, 648 (2008).
13. J. R. Maze, P. L. Stanwix, J. S. Hodges, S. Hong, J. M. Taylor, P. Cappellaro, L. Jiang, M. V. G. Dutt, E. Togan, A. S. Zibrov, A. Yacoby, R. L. Walsworth and M. D. Lukin, Nature **455**, 644 (2008).
14. V. Pardo and W. Pickett, Phys. Rev. Lett. **102**, 166803 (2009).
15. W. Ren, T. H. Cho, T. C. Leung and C. T. Chan, Appl. Phys. Lett. **93**, 142102 (2008).
16. K. Seino, W. Schmidt and F. Bechstedt, Phys. Rev. Lett. **93**, 036101 (2004).
17. P. Tamarat, N. B. Manson, J. P. Harrison, R. L. McMurtrie, A. Nizovtsev, C. Santori, R. G. Beausoleil, P. Neumann, T. Gaebel, F. Jelezko, P. Hemmer and J. Wrachtrup, New J. Phys. **10**, 045004 (2008).
18. P. Tamarat, T. Gaebel, J. Rabeau, M. Khan, A. Greentree, H. Wilson, L. Hollenberg, S. Prawer, P. Hemmer, F. Jelezko and J. Wrachtrup, Phys. Rev. Lett. **97**, 083002 (2006).
19. E. Van Oort and M. Glasbeek, Chem. Phys. Lett. **168**, 529 (1990).
20. F. Dolde, H. Fedder, M. W. Doherty, T. Nöbauer, F. Rempp, G. Balasubramanian, T. Wolf, F. Reinhard, L. C. L. Hollenberg, F. Jelezko and J. Wrachtrup, Nat. Phys. **7**, 459 (2011).
21. L. T. Sun, J. L. Gong, Z. Y. Zhu, D. Z. Zhu, Z. X. Wang, W. Zhang, J. G. Hu and Q. T. Li, Diam. Relat. Mater. **14**, 749 (2005).
22. S. A. Rakha, Y. Guojun, Z. Xingtai, I. Ahmed, D. Zhu and J. Gong, J. Cryst. Growth **311**, 3332 (2009).
23. Y. Ando, Y. Nishibayashi and A. Sawabe, Diam. Relat. Mater. **13**, 633 (2004).
24. E. S. Baik, Y. J. Baik, S. W. Lee and D. Jeon, Thin Solid Films **377-378**, 295 (2000).
25. B. Wen, J. Zhao and T. Li, Chem. Phys. Lett. **441**, 318 (2007).
26. A. S. Barnard and I. K. Snook, J. Chem. Phys. **120**, 3817 (2004).

27. C. Zhuang, X. Jiang, J. Zhao, B. Wen and X. Jiang, Physica E **41**, 1427 (2009).
28. X. Jiang, J. Zhao and X. Jiang, Nanotechnology **22**, 405705 (2011).
29. A. S. Barnard, S. P. Russo and I. K. Snook, Nano Lett. **3**, 1323 (2003).
30. G. Kresse and D. Joubert, Phys. Rev. B **59**, 1758 (1999).
31. J. Heyd, G. E. Scuseria and M. Ernzerhof, J. Chem. Phys. **118**, 8207 (2003).
32. J. P. Perdew, M. Ernzerhof and K. Burke, J. Chem. Phys. **105**, 9982 (1996).
33. J. Bang, Y. Y. Sun, T. A. Abtew, A. Samanta, P. Zhang and S. B. Zhang, Phys. Rev. B **88**, 035134 (2013).
34. M. E. Straumanis and E. Z. Aka, J. Am. Chem. Soc. **73**, 5643 (1951).
35. P. Denham, E. C. Lightowlers and P. J. Dean, Phys. Rev. **161**, 762 (1967).
36. H. J. Monkhorst and J. D. Pack, Phys. Rev. B **13**, 5188 (1976).
37. M. Methfessel and A. Paxton, Phys. Rev. B **40**, 3616 (1989).
38. J. Neugebauer and M. Scheffler, Phys. Rev. B **46**, 16067 (1992).
39. L. Bengtsson, Phys. Rev. B **59**, 12301 (1999).
40. S. Saha, T. P. Sinha and A. Mookerjee, Phys. Rev. B **62**, 8828 (2000).
41. T. Abtew, Y. Sun, B.-C. Shih, P. Dev, S. Zhang and P. Zhang, Phys. Rev. Lett. **107**, 146403 (2011).
42. P. Mahadevan and S. Mahalakshmi, Phys. Rev. B **73**, 153201 (2006).
43. O. Volnianska and P. Boguslawski, J. Phys: condens. Mat. **22**, 073202 (2010).
44. J. R. Maze, P. L. Stanwix, J. S. Hodges, S. Hong, J. M. Taylor, P. Cappellaro, L. Jiang, M. V. Dutt, E. Togan, A. S. Zibrov, A. Yacoby, R. L. Walsworth and M. D. Lukin, Nature **455**, 644 (2008).
45. P. Dev, Y. Xue and P. Zhang, Phys. Rev. Lett. **100**, 117204 (2008).
46. R. F. W. Bader, *Atoms in Molecules: A Quantum Theory*. (International Series of Monographs on Chemistry, Clarendon,Oxford, 1990).
47. A. Beveratos, R. Brouri, T. Gacoin, J.-P. Poizat and P. Grangier, Phys. Rev. A **64**, 061802 (2001).
48. B. J. M. Hausmann, M. Khan, Y. Zhang, T. M. Babinec, K. Martinick, M. McCutcheon, P. R. Hemmer and M. Lončar, Diam. Relat. Mater. **19**, 621 (2010).
49. I. Friedler, C. Sauvan, J. P. Hugonin, P. Lalanne, J. Claudon and J. M. Gérard, Opt. Express **17**, 2095 (2009).
50. T. M. Babinec, J. M. HausmannBirgit, M. Khan, Y. Zhang, J. R. Maze, P. R. Hemmer and M. Loncar, Nat. Nano. **5**, 195 (2010).

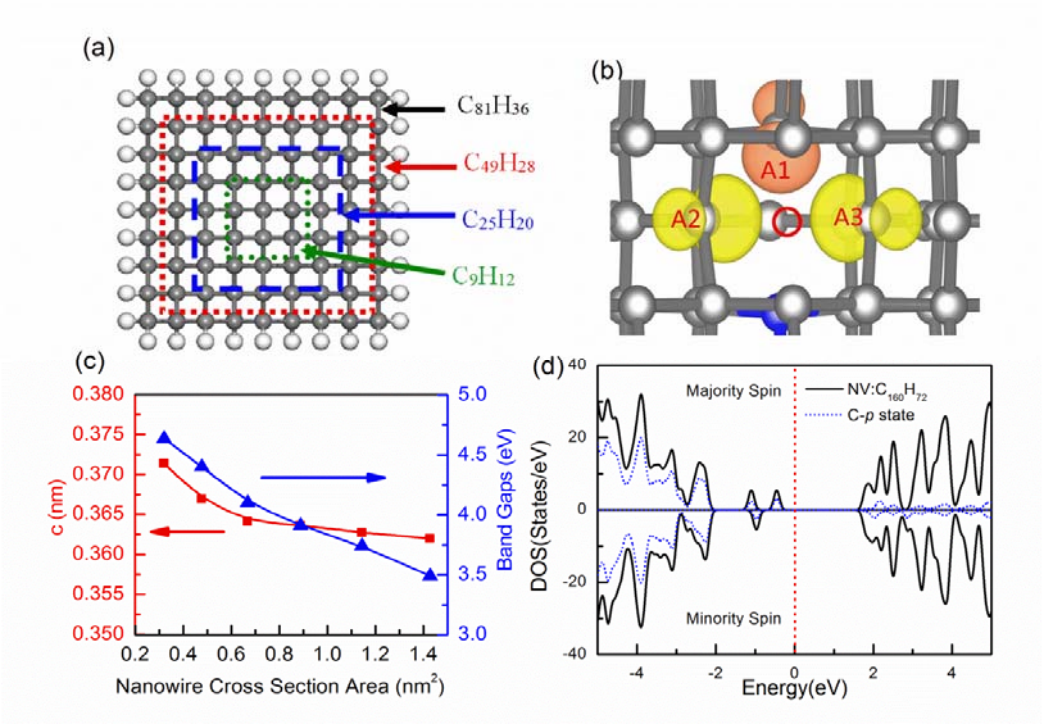

Fig. 1 (Color online) (a) The cross section of the hydrogenated diamond nanowires with C{100} surface. (b) Isosurface charge density plot (with an isovalue ρ = 0.02 e/Å^3) of the spin states for NV:$C_{160}H_{72}$, showing the localized nature of defect states. C: gray; N: blue; C vacancy: red circle. (c) Lattice constants *c* (red square) and electronic band gap (blue triangle) v.s. the cross-sectional area of hydrogenated diamond nanowires. (d) DOS of NV:$C_{160}H_{72}$ (black). The upper and lower panels of the DOS represent majority- and minority-spin channels, respectively. The blue dotted lines represent C-2*p* states of NV:$C_{160}H_{72}$. The Fermi level is indicated by the vertical dash line.

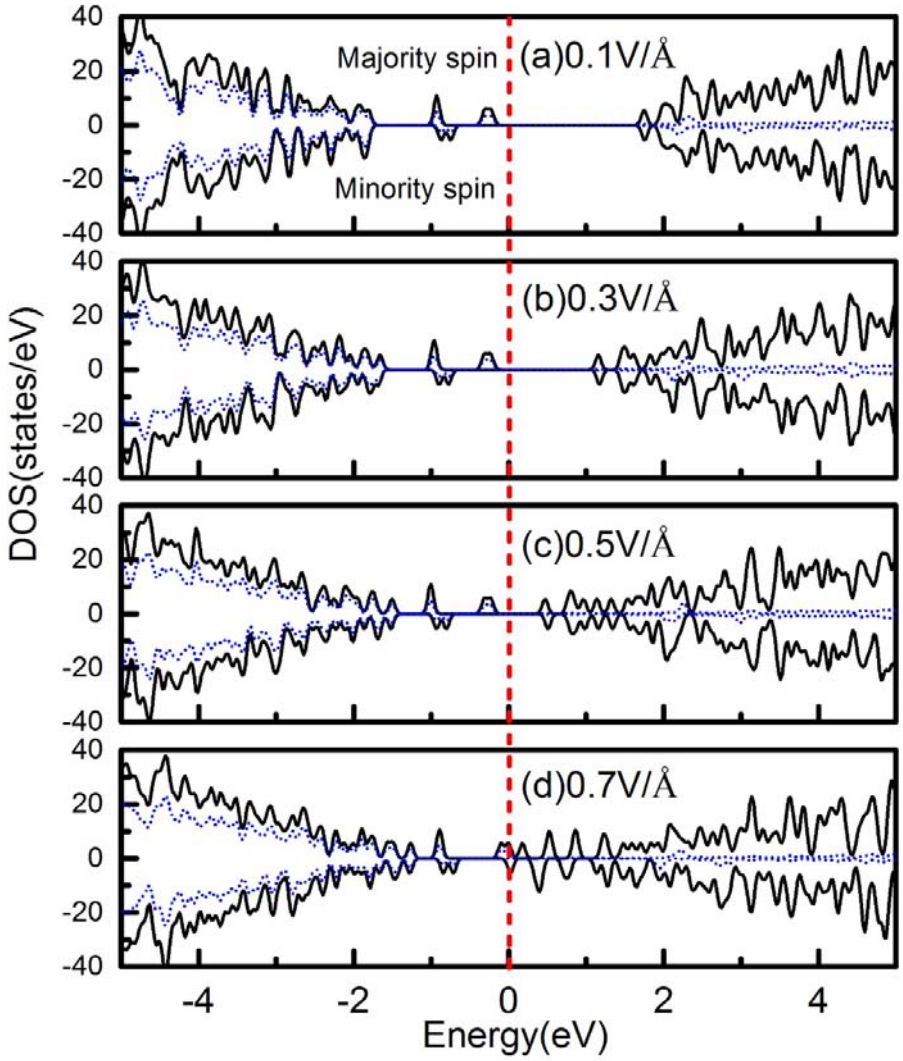

Fig. 2 (a-d) DOS of NV:$C_{160}H_{72}$ under external electric fields $\vec{E}$ of 0.1, 0.3, 0.5, 0.7 V/Å. The blue dotted lines show projections of the DOS onto C-2*p* states. The upper and lower panels of each DOS plot represent the majority- and minority-spin channels, respectively. The Fermi level is indicated by the vertical dash line.

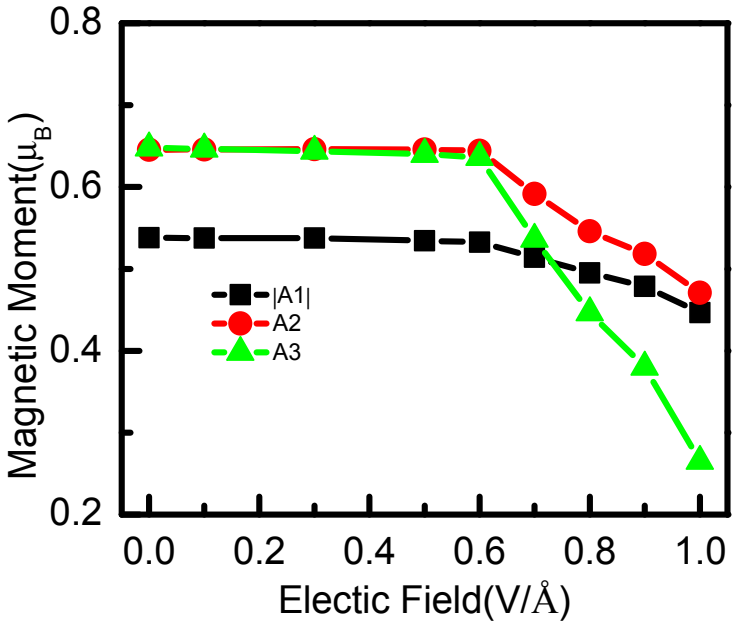

Fig. 3 Local magnetic moments of A1, A2 and A3 atoms as a function of the external electric field $\vec{E}$.

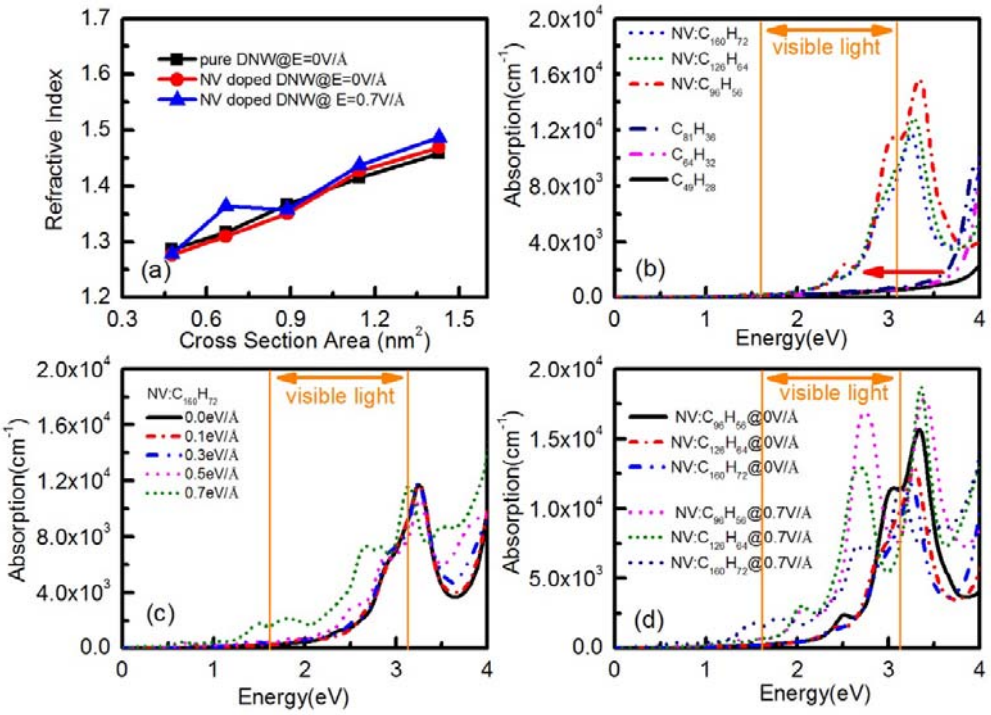

Fig. 4 (Color online) (a) The refractive index vs nanowire cross section area of the hydrogenated DNW under external electric fields $\vec{E}$ of 0 and 0.7V/Å. (b) Absorption coefficients of $C_{49}H_{28}$, $C_{64}H_{32}$, $C_{81}H_{36}$, $NV:C_{96}H_{56}$, $NV:C_{128}H_{64}$ and $NV:C_{160}H_{72}$ without external electric field. (c) Absorption coefficients of $NV:C_{160}H_{72}$ under external electric fields $\vec{E}$ of 0, 0.1, 0.3, 0.5, 0.7 V/Å. (d) Absorption coefficients of $NV:C_{96}H_{56}$, $NV:C_{128}H_{64}$ and $NV:C_{160}H_{72}$ under $\vec{E}$ = 0 and 0.7 V/Å.